

Detonation of an Explosive Containing Carbon Nanotubes

A. P. Ershov^a, G. R. Dashapilov^{a,b}, D. I. Karpov^{a,b},
A. O. Kashkarov^{a,b}, Ya. L. Luk'yanov^a,
E. R. Prueel^{a,b}, and I. A. Rubtsov^{a,b}

UDC 662.215.1

Published in *Fizika Goreniya i Vzryva*, Vol. 57, No. 1, pp. 112–119, January–February, 2021.
Original article submitted October 29, 2019; revision submitted December 17, 2019; accepted for publication December 24, 2019.

Abstract: RDX containing a small amount of single-walled carbon nanotubes is obtained by the method of co-precipitation out of a solution. The detonation of this composition is studied by an electromagnetic method of mass velocity measurement and by a high-resolution electroconductivity method. A clearly expressed chemical spike is observed. Preliminary indications of reaction acceleration in the presence of nanotubes are obtained. The electroconductivity measurements are complicated because of the noticeable conductivity of the original material; if this factor is taken into account, the electrical conductivity profiles behind the detonation front are similar to those observed for pure RDX. Possible reasons for the influence of nanotubes on detonation characteristics are discussed.

Keywords: detonation, explosion, carbon nanotubes.

DOI: 10.1134/S0010508221010123

INTRODUCTION

Intense application of carbon nanotubes (CNTs) in various fields of engineering is observed in recent years. The unique properties of CNTs (high longitudinal conductivity and very large ratio of their length to diameter) are responsible for the noticeable electrical conductivity of mixtures arising already when CNT addition is at a level of hundredths fractions of a percent. It can be also expected that this new material will be useful as an additive to high explosive (HEs). A positive effect of providing the electrical conductivity in a composite with the corresponding reduction of electrization is obvious. At the same time, addition of nanotubes can modify the detonation characteristics of the HE. As far as the authors are aware, this aspect has not been studied yet.

Fairly efficient methods of CNT production were developed; as a result, their cost decreased to a level that allows CNTs to be considered as an additive to explosive materials. According to information available now, single-walled carbon nanotubes (SWCNTs) ensure almost safe operation. In particular, TUBALL nanotubes produced by the OCSiAl company in Novosibirsk became the first SWCNTs registered in accordance with the European Union's Registration, Evaluation, Authorization, and Restriction of Chemicals (REACH) regulations, and their industrial-scale production is allowed (see/https://en.wikipedia.org/wiki/Carbon_nanotube).

In the present study, we consider the influence of addition of small amounts of CNTs on the detonation properties of RDX.

PREPARATION OF SPECIMENS

The study was performed with TUBALL COAT E single-walled nanotubes produced by the OCSiAl company. The characteristic length of these nanotubes was several micrometers, and their diameter was approximately 1.5 nm. The RDX solution in acetone was mixed

^aLavrent'ev Institute of Hydrodynamics, Siberian Branch, Russian Academy of Sciences, Novosibirsk, 630090 Russia; ers@hydro.nsc.ru.

^bNovosibirsk State University, Novosibirsk, 630090 Russia.

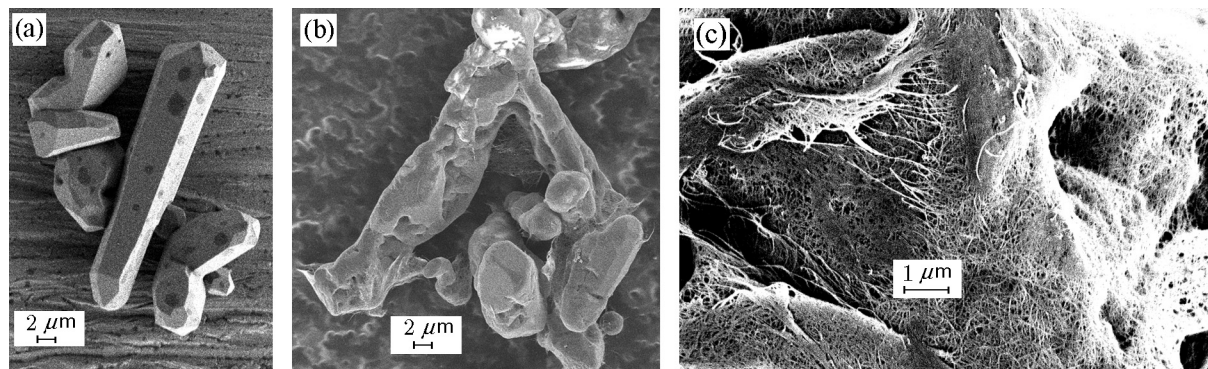


Fig. 1. SEM images of HE particles: high-purity fine-grained RDX (a) and RDX + 0.5% of SWCNTs with different magnifications (b and c).

with the aqueous solution of 0.2% of SWCNTs, after which both RDX and SWCNTs precipitated, and the sediment was dried. High-purity fine-grained RDX was prepared in the same way, except for addition of SWCNTs. Figure 1 shows the images obtained by scanning electron microscopy (SEM) with a LEO-420 microscope.

As nanotubes can act as crystallization centers, it was expected that addition of SWCNTs would reduce the HE particle size. However, the sizes of pure HE grains and RDX particles in the mixture with SWCNTs were found to be approximately identical (Figs. 1a and 1b). Nevertheless, the materials were seen to be noticeably different. Pure RDX formed crystals with clearly expressed faceting, whereas the grains in the mixture with SWCNTs were rounded and contained pores of micron and submicron sizes (Figs. 1b and 1c). The majority of nanotubes surrounded the HE particles, though some of them could penetrate inward the grains and act like “reinforcement.” The dried powder had a dark gray color and did not display any noticeable electrization owing to composite conductivity. In contrast to micron and submicron powders of pure HE, the material was not prone to formation of a suspension in air; therefore, it was not difficult to work with it.

MASS VELOCITY MEASUREMENTS

The variant of electromagnetic diagnostics used in the present study was described in detail in [2]. The material was pressed in the form of cylindrical charges 20 mm in diameter and 14–20 mm long. Identical charges of pure RDX were also prepared for comparisons. II-shaped sensors made of aluminum 9 μm thick with the working arm length of about 1 mm were used, which made it possible to work with charges of comparatively small diameters. The sensor was placed on a

Plexiglas block 8 mm thick and was separated from the end face of the cylindrical HE charge by a protective epoxy layer 50–100 μm thick. The charge was initiated at the opposite end face by a detonator through a small-size generator of the plane wave. A pulsed magnetic field $B = 0.15$ T was generated by the Helmholtz coil. The time resolution was approximately 5 ns.

The pressed charges of pure HE fell into pieces easily (sometimes, just in hands). Therefore, RDX specimens were pressed at the maximum reachable pressure (which corresponded to the density of 1.7 g/cm^3), but special care had to be applied in this case. If SWCNTs were added, the material compressibility decreased, and the same force of the pressing device ensured the density of 1.62 g/cm^3 . The charges with SWCNT addition had a smaller density, but a sufficient strength. Obviously the nanotubes played the role of a binder. According to [3], for the RDX density of 1.7 g/cm^3 , the mass velocity and pressure in the Chapman–Jouguet (CJ) state were $u = 2.063$ km/s and $p = 29.44$ GPa; the corresponding values for the density of 1.62 g/cm^3 were $u = 1.975$ km/s and $p = 26$ GPa. As the mass fraction of nanotubes was small, their influence on the level of the CJ parameters could be ignored.

The experimentally recorded curves of the velocity of the HE–Plexiglas interface are shown in Fig. 2. The results of two tests are given for each composition. The oscillations before the beginning of the main signal (at $t < 0$) are caused by matter polarization in the vicinity of the wave front. In the pressed material, these interferences are small and do not affect the subsequent profile.

As is seen from Fig. 2, the reproducibility of the tests is better for pure HE. Apparently, the SWCNT distribution in the material was not sufficiently homogeneous after our preparation procedure, which could affect the structure and local density of the charge.

The chemical spike was observed in all experiments: the maximum velocity of the interface was obviously greater than the CJ state predictions. For brevity, this line indicates the velocity of the interface between the window and HE, which is reached after unloading of detonation products from the CJ state of RDX. Figure 2 shows the CJ levels calculated on the basis of the above-mentioned states of detonation products and the shock adiabat of Plexiglas from [4]. For pure RDX, the ratio of the spike velocity to the CJ level is close to 1.4. An almost the same ratio was obtained for RDX with nanotubes in test No. 41, but its value in test No. 43 was 1.18. The reasons for this reduction of the chemical spike amplitude could be local inhomogeneity and, possibly, partial reaction during the first nanoseconds, which is also associated with inhomogeneity of the material.

In all experiments, the interface velocity profiles did not display any obvious specific features that could be interpreted as the end of the reaction. With certain caution, the kinetics can be estimated on the basis of the chemical spike length defined as the time interval needed to reach the CJ level. In the case of smooth completion of the reaction, this value can be overestimated by several times [5, 6] even in simulations of the process where all parameters are known exactly. In real experiments, both experimental scatter and inaccuracy in determining the CJ level are possible. In contrast to previous studies [2, 7], HE unloading occurs from states located rather far from the shock adiabat on the $p-u$ diagram because of the higher HE density, which reduces the simulation accuracy. As is seen from Fig. 2, a small error in determining the CJ level can significantly change the reaction time estimate. Moreover, the effect of data scattering is so high that the CJ level was not reached at all in one of the experiments with pure RDX within reasonable time.

Nevertheless, it can be expected that comparisons of experiments performed under identical conditions can reveal the influence of SWCNT addition. With allowance for previous comments, Fig. 2 manifests certain reduction of the chemical spike length in the composition containing nanotubes. More definite conclusions require additional investigations.

MEASUREMENTS OF ELECTRICAL CONDUCTIVITY

Investigations of electrical conductivity in the vicinity of the detonation front allows one to obtain more useful information in addition to dynamic measurements. This approach seems to be particularly suit-

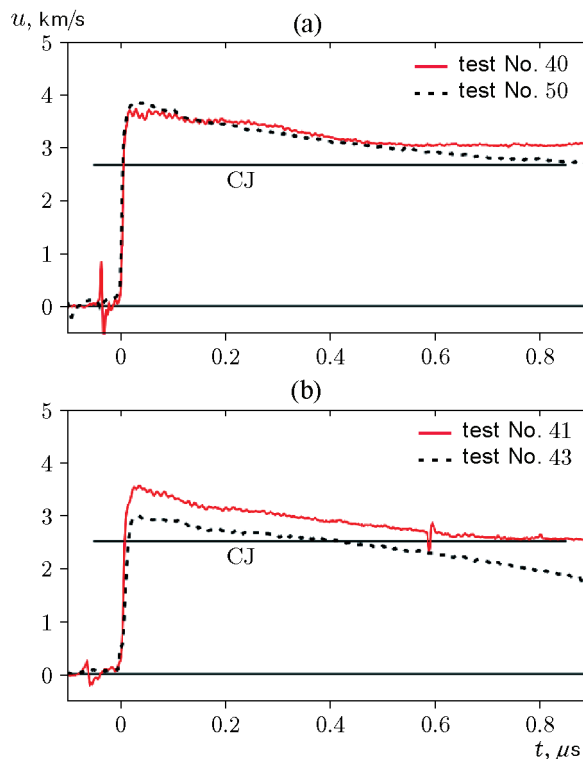


Fig. 2. Effect of SWCNTs on the interface velocity in the case of RDX detonation: (a) pure RDX with the initial density of 1.7 g/cm^3 ; (b) RDX + 0.5% of SWCNTs with the initial density of 1.62 g/cm^3 ; the lines indicated as CJ show the predicted levels of the interface boundary in the CJ state.

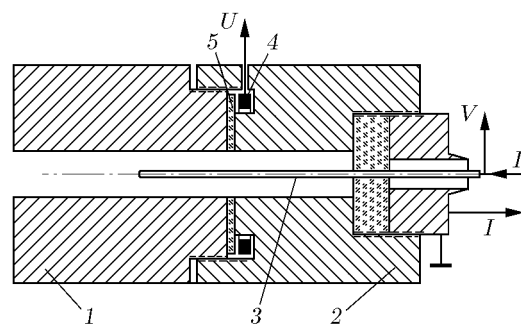


Fig. 3. Electrical conductivity cell.

able for initially conducting substances. The method of measuring the electrical conductivity profile in the detonation wave was described in [8, 9]. As the measurements in initially conducting materials have some specific features, we provide a brief description of the measurement cell.

We used a coaxial system of electrodes shown in Fig. 3. The charge with the diameter $b = 8 \text{ mm}$ was pressed into a thick copper shell whose parts 1 and 2

were connected by threading. The external diameter of the shell was 40 mm. The axial copper electrode 3 (diameter $c = 2$ mm, length of the region inside the HE 30 mm) was placed in a Plexiglas plug fixed by a hollow bolt. The sensor for measuring electrical conductivity 4 was a toroidal coil located in the cavity of the external electrode. The coefficient of mutual induction of the coil and cavity circuit was $M \approx 15$ nH. The width of the slit connecting the cavity with the coaxial was defined by the dielectric layer 5 (in our experiments, polypropylene 0.3 or 0.6 mm thick).

The pulsed current I feeding the cell was generated by a special external power source. In contrast to previous studies [8, 9], the cell was filled by an initially conducting material. The resistance of the cell was 1.4Ω for the HE density of 1.6 g/cm^3 and 1.1Ω for the HE density of 1.8 g/cm^3 for the current of about 1 mA (the measurements were performed by a Keysight 34461A multimeter). This corresponds to the static electrical conductivity of $0.05\text{--}0.07 \Omega^{-1} \cdot \text{cm}^{-1}$. However, the resistance decreased to 0.19Ω (1.6 g/cm^3) and 0.14Ω (1.8 g/cm^3) when the electrical conductivity was measured in the course of detonation for the current through the cell approximately equal to 40 A, i.e., the conductivity increased by an order of magnitude: up to $0.4\text{--}0.5 \Omega^{-1} \cdot \text{cm}^{-1}$. It can be assumed that new conducting channels are involved as the electric field is enhanced.

Initially, the current in the cell is distributed between parts 1 and 2 of the external shell. The current portion arriving at the electrode 1 flows around the sensor cavity, thus, generating a magnetic flux in the coil 4. The detonation wave is initiated at the left end face of the charge and moves to the right with a velocity D . When the wave reaches the axial electrode, the resistance of the medium in the left part of the cell starts to change, which affects the current in this part and the magnetic flux in the coil winding. As a result, there arises a signal on the coil (which is not large in practice of our measurements). Later, when the wave front passes near the slit, some portion of the current is switched to the external electrode 2. The current passing through the cavity and the magnetic flux decrease, generating the main voltage pulse of the sensor U . For a steady profile of electrical conductivity behind the wave after this instant, the electrical conductivity in the plane of the slit is proportional to $U(t)$:

$$\sigma(x) = \frac{\ln(b/c) U(t)}{2\pi DM V}. \quad (1)$$

Here $x = Dt$ is the distance covered by the wave front moving away from the slit by the time t and V is the voltage on the central electrode. Formula (1) is valid if the slit is thin (as compared to the width of the con-

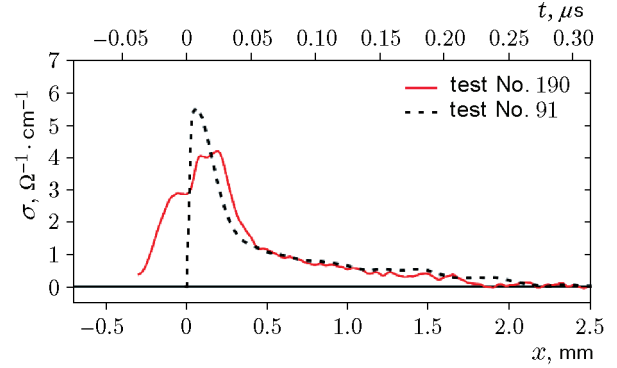


Fig. 4. Profiles of electrical conductivity behind the detonation front: the slit width is 0.3 mm; the solid and dashed curves show the results for RDX + 0.5% of SWCNTs (1.6 g/cm^3) and for pure RDX of the same density.

ducting region behind the wave front). The influence of the finite width of the slit will be considered below.

The results of experiments with RDX containing 0.5% of SWCNTs are illustrated in Fig. 4, which also shows the profile of electrical conductivity in pure RDX obtained previously.

The profile for the composition with nanotubes is shifted to the left in order to superimpose the regions of the distribution peaks and the subsequent decrease of the curves. After that, at $t > 0$, reasonable agreement between the two profiles is reached. However, the curve for the composition with nanotubes also displays a “precursor,” i.e., at first glance, the presence of nanotubes leads to significant widening of the profile. As is shown below, the region of the curve at $t < 0$ does not reflect the real conductivity behind the wave front; it arises owing to specific features of current spreading in the cell, which are associated with the finite electrical conductivity of the medium ahead of the front. Thus, within the framework of accuracy of our measurements, the presence of nanotubes does not produce any noticeable effect on the electrical conductivity distribution behind the detonation front. Similar results were obtained for the higher charge density of 1.8 g/cm^3 .

The slit width (0.3 mm) is comparable with the characteristic width of the electrical conductivity profile. Therefore, distortions are possible in the peak region. For a narrower slit, the distortions are smaller, but rapid closure of the electrodes 1 and 2 occurs above the dielectric, and the signal vanishes. It is seen from Fig. 4 that the closure occurs in $0.22\text{--}0.27 \mu\text{s}$ for the slit width of 0.3 mm. Thus, these experiments were performed at the limit of the method capabilities.

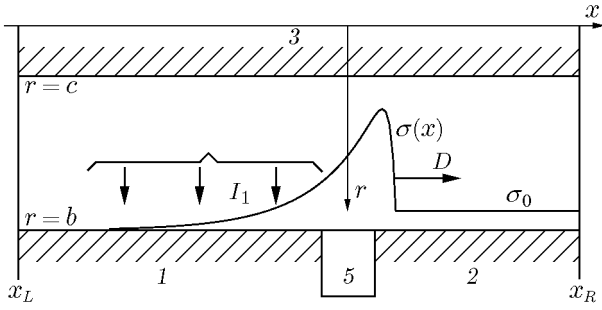


Fig. 5. Simulation geometry.

MODELING OF THE CELL

To estimate the influence of the initial conductivity on the measurements, we performed large-scale simulations of the current distribution in the cell and the sensor response. A two-dimensional axisymmetric problem in a real geometry was solved. The computational domain is schematically shown in Fig. 5. The x axis coincides with the cell axis; the electrodes and dielectric are indicated in the same way as those in Fig. 3. The radial coordinate changes from $r = c = 1$ mm to $r = b = 4$ mm. A steady wave of electrical conductivity moves along the cell; the figure shows its position at a certain time instant. A constant initial electrical conductivity σ_0 may exist ahead of the wave.

We solved the equation

$$\frac{1}{r} \frac{\partial}{\partial r} \left(r \sigma \frac{\partial \varphi}{\partial r} \right) + \frac{\partial}{\partial x} \left(\sigma \frac{\partial \varphi}{\partial x} \right) = 0, \quad (2)$$

where φ is the electric field potential, and the electrical conductivity σ is a function of the longitudinal coordinate x . The boundary conditions are $\varphi = 0$ at $r = b$, $x_L \leq x < -a/2$, and $a/2 < x \leq x_R$, i.e., on the external electrode, $\varphi = 1$ at $r = c$ (on the central electrode), $\frac{\partial \varphi}{\partial r} = 0$ at $r = b$, $-a/2 \leq x \leq a/2$ and $\frac{\partial \varphi}{\partial x} = 0$ at $x = x_L$ and $x = x_R$. Here $a = 0.3$ mm is the thickness of the dielectric 5, while x_L and x_R are the left and right boundaries of the computational domain, which are located at sufficient distances from the region of field inhomogeneity (dielectric surface). The coordinate $x = 0$ corresponds to the middle of the dielectric layer.

The electrical conductivity of the medium in the case of an initially non-conducting material is defined by the following formulas:

for $x < x_0$,

$$\sigma(x) = A \exp(k_1(x - x_0))(1 - \exp(k_2(x - x_0))); \quad (3)$$

for $x \geq x_0$, $\sigma(x) = 0$.

Here x_0 is the position of the electrical conductivity wave front. The coefficients k_1 and k_2 were chosen to ensure an approximate description of the electrical conductivity distribution in pure HE, which had the characteristic fall length $1/k_1 \approx 0.6$ mm and a comparatively sharp front ($k_2 = 10k_1$).

If there was some initial conductivity $\sigma_0 > 0$, the wave front position did not coincide with x_0 ; instead, it was determined by intersection of curve (3) and horizontal line $\sigma(x) = \sigma_0$. In fact, the front coordinate was defined at the computational grid node, and the value of x_0 was found numerically.

Equation (2) was solved by the relaxation method with simple iterations on a square grid in the above-indicated domain. The simulations were performed by a specially developed program for the graphical processing unit using parallel algorithms based on the CUDA technology. The criterion of convergence of the algorithm was the condition of equality of the current I_c leaving the central electrode and the current I_b collected on the external electrode:

$$I_c = -2\pi c \int_{x_L}^{x_R} \sigma \frac{\partial \varphi}{\partial r} dx, \quad I_b = -2\pi b \int_{x_L}^{x_R} \sigma \frac{\partial \varphi}{\partial r} dx.$$

The computation was terminated when the normalized error $|(I_b - I_c)/I_b|$ became smaller than $2 \cdot 10^{-6}$. For grids up to 512×2048 nodes in size, the duration of one computation with such an error was 15–20 min. Such grid corresponded to division of the dielectric region of the boundary into 51 interval, which seems to be sufficiently detailed partitioning.

These simulations were performed many times for different positions of the front of the electrical conductivity distribution, which corresponded to detonation wave motion. The parameter stored after each simulation was the current I_1 collected on the electrode 1:

$$I_1 = -2\pi b \int_{x_L}^{-a/2} \sigma \frac{\partial \varphi}{\partial r} dx.$$

In the experiments, the signal of the coil 4 is proportional to the derivative of the current $-\frac{dI_1}{dt}$ (the minus is used because I_1 decreases after reaching the slit).

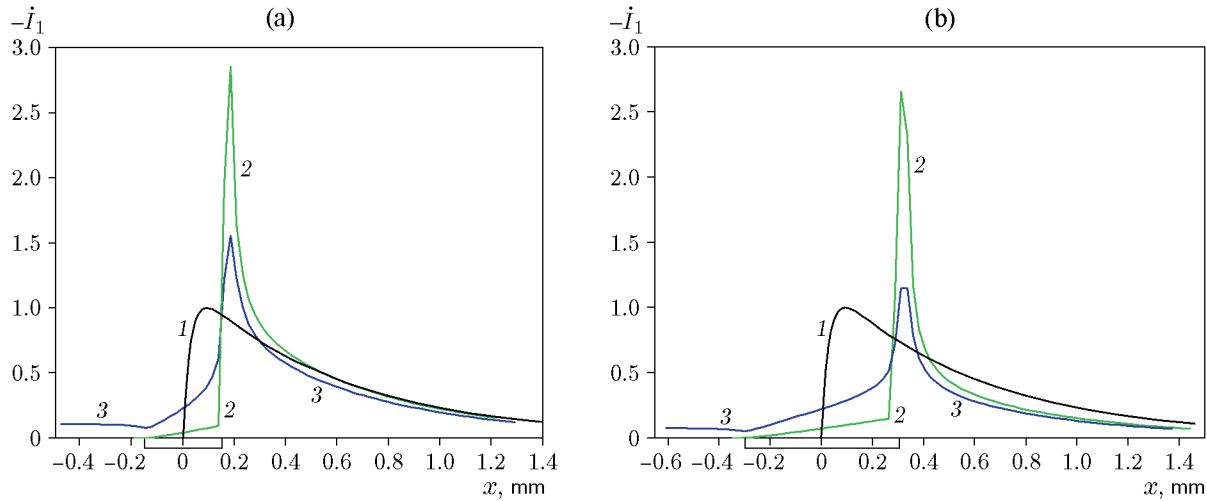


Fig. 6. Simulation results: (a) slit width 0.3 mm; (b) slit width 0.6 mm; curve 1 shows the specified profile of electrical conductivity (for $\sigma_0 = 0$) and curves 2 and 3 are the scaled derivatives $-\dot{I}_1$ for $\sigma_0 = 0$ and 0.125, respectively.

In the simulations, this corresponds to the derivative $-\dot{I}_1$ with respect to the front coordinate with appropriate scaling. The results of simulations for the unit amplitude of the electrical conductivity distribution are shown in Fig. 6.

The thickness of the dielectric in Fig. 6a is 0.3 mm, which is half of the characteristic fall length of electrical conductivity. The dielectric position is marked by a rectangle under the abscissa axis. The calculated curve 2 begins immediately after the wave reaches the dielectric because some part of the conducting region no longer contacts the electrode 1, which somewhat increases the resistance of the cell and decreases the current I_1 . Such a weak “precursor” was indeed observed in some experiments, though it could be missed against the background of experimental noise. An intense peak is observed at the instant when the front reaches the electrode 2 because a noticeable portion of the current is switched to this electrode (the electric field has a singularity at the corner point $r = b$, $x = a/2$). However, this distortion of the signal soon becomes smaller. For example, at $x = 0.3$ mm, the excess of the level above the true value is approximately 20%, which can be estimated as acceptable accuracy for experiments with explosives. At $x = 0.4$ mm, the error decreases to 6%, and the curves almost coincide at $x > 0.4$ mm. Simply speaking, the distortion of the field in the vicinity of the dielectric reduces the measured profile approximately by one half of the dielectric layer width, while

the area under the curve remains unchanged.

Noticeable initial electrical conductivity (1/8 part of the maximum value for Fig. 6, which approximately corresponds to the experimental data in Fig. 4) changes the character of profile distortion. Namely, the precursor on curve 3 is expressed more clearly. When the front passes through the slit region, some portion of the current branches off to the electrode 2, resulting in marked reduction of the current I_1 . Vice versa, the excess of the peak becomes less sharp. Such results are natural because the presence of noticeable initial electrical conductivity can be treated as some smoothing of the electrical conductivity distribution.

For the doubled width of the slit (0.6 mm), the response of the cell reflects the real distribution of electrical conductivity rather poorly, though the curves far from the dielectric are qualitatively consistent (Fig. 6b). Note that the error of the maximum amplitude of the signal is significantly smaller for the conducting composition in both simulation variants.

The simulation results described here can be considered as justification of the conclusion about the absence of any significant influence of nanotubes on the electrical conductivity profile, which was made in the previous paragraph. Indeed, Fig. 4 shows the precursor, which is exactly 0.3 mm wide, followed by the main peak. The relationship of the curves for the initially conducting material and pure RDX is consistent with the model computations.

CONCLUSIONS

A procedure of preparing RDX with addition of 0.5% of single-walled carbon nanotubes was proposed; the productivity was sufficient for subsequent dynamic measurements. It was demonstrated that charges can be pressed without any binders. The resultant material ensured electrical conductivity at a level of $0.05\text{--}0.5\ \Omega^{-1}\cdot\text{cm}^{-1}$, and the resistance of the specimens decreased with an increase in the current density.

The detonation wave structure was studied with the use of two diagnostic tools: by means of electromagnetic measurements of mass velocity and by the electroconductivity method. The latter is significantly affected by the initial conductivity of the material. Simulations of current spreading in the coaxial cell ensured a correct interpretation of experimental data.

The electromagnetic measurements indicated that SWCNT addition exerts a certain effect on the reaction kinetics. The reason for this effect can be the change in the substance structure. RDX condensation in the presence of nanotubes leads to the formation of porous particles. In the pressing process, nanotubes surrounding HE grains prevent the total collapse of gaps between the grains. Multiple pores can act as nuclei of hot spots. It is also possible that nanotubes favor spreading of the reaction owing to the high thermal conductivity.

Nanotubes produce practically no effect on the electrical conductivity profile, which is apparently caused by their rapid destruction in the wave front. Indeed, shock wave experiments [10] showed that SWCNTs start to destroy already at a pressure of 19 GPa, which is much lower than the CJ pressure in RDX with the density of $1.6\ \text{g}/\text{cm}^3$. Complete destruction of SWCNTs is observed at 36 GPa. This value approximately corresponds to the pressure in the Neumann spike. According to [11], the majority of single-walled carbon nanotubes are destroyed already at 26 GPa. Under the detonation wave conditions, at temperatures of several thousand Kelvins, the destruction process is expected to be even more intense. After that, the mechanism of electrical conductivity does not differ from that in the pure HE. Based on experimental profiles, the SWCNT destruction time can be estimated as 10 ns or smaller.

Thus, SWCNT addition ensures some advantages of explosives: there is no electrization, and the material is pressed without any additional binders. Concerning the influence on the detonation characteristics, the main role of nanotubes seems to be the modification of the initial distribution of HE porosity.

Because of comparatively small sizes of the examined charges, the measured velocities can be underestimated as compared to the ideal values. According to

our estimates, the influence of the diameter for such an active substance as RDX is insignificant. For example, the detonation velocity obtained for charges 12–15 mm in diameter [12] with due allowance for the small difference in density practically coincides with the velocity measured in [13] for the diameter of 40 mm. The finite length of the charges can also affect the wave parameters, but this drawback is partly compensated by the plane-wave initiator. The values of the measured mass velocity within the accuracy of our experiment are consistent with the expected values, which implies that the scaling factor produces a minor effect.

The authors are grateful to N. P. Satonkina for her kind assistance in the experiment and useful discussions.

This work was partly supported by the Russian Foundation for Basic Research (Grant No. 18-03-00441).

REFERENCES

1. A. V. Eletsii, A. A. Knizhnik, B. V. Potapkin, and Kh. M. Kenni, "Electrical Characteristics of Polymer Composites Containing Carbon Nanotubes," *Usp. Fiz. Nauk* **185** (3), 225–270 (2015).
2. A. P. Ershov and I. A. Rubtsov, "Detonation of Low-Density Explosives," *Fiz. Goreniya Vzryva* **55** (1), 128–135 (2019) [*Combust., Expl., Shock Waves* **55** (1), 114–120 (2019)]; 10.1134/S0010508219010131.
3. K. Tanaka, "Detonation Properties of Condensed Explosives Computed using the Kihara–Hikita–Tanaka Equation of State," in *Tech. Report Nat. Chem. Lab. for Industry, Tsukuba Research Center* (Tsukuba, Japan, 1983).
4. W. J. Carter and S. P. Marsh, "Hugoniot Equation of State of Polymers," Report No. LA-13006-MS (Los Alamos National Laboratory, Los Alamos, 1995).
5. S. M. Bakhraikh, A. A. Evstigneev, V. N. Zubarev, and A. A. Shanin, "Influence of the Finite Rate of High-Explosive Decomposition on the Determination of Detonation Parameters," *Fiz. Goreniya Vzryva* **17** (6), 117–121 [*Combust., Expl., Shock Waves* **17** (6), 685–6868 (1981)].
6. A. P. Ershov, "Regimes of Detonation of Solid Explosives with Nonclassical Fast Kinetics," *Fiz. Goreniya Vzryva* **49** (3), 77–87 (2013) [*Combust., Expl., Shock Waves* **49** (3), 325–334 (2013)].
7. A. P. Ershov, A. O. Kashkarov, E. R. Prueel, et al., "Nonideal Detonation Regimes in Low Density Explosives," *J. Appl. Phys.* **119** (7), 075903 (2016).
8. A. P. Ershov, N. P. Satonkina, and G. M. Ivanov, "Profiles of Electrical Conductivity in Dense Explosives," *Khim. Fiz.* **26** (12), 21–33 (2007).

9. A. P. Ershov and N. P. Satonkina, "Electrical Conductivity Distributions in Detonating Low-Density Explosives—Grain Size Effect," *Combust. Flame* **157** (5), 1022–1026 (2010).
10. M. Noël, S. Ananev, M. Mases, et al., "Probing Structural Integrity of Single Walled Carbon Nanotubes by Dynamic and Static Compression," *Phys. Status Solidi Rapid Res. Lett.* **8** (11), 935–938 (2014).
11. S. Yu. Anan'ev, "Physical and Chemical Transformations of Carbon Nanostructures and Reaction Capable Mixtures under Shock Wave Actions," Candidate's Dissertation (Joint Inst. for High Temp., Russian Acad. of Sci., Moscow, 2018).
12. I. N. Aizenshtadt, "A Method of Calculating the Ideal Detonation Velocity of Condensed Explosives," *Fiz. Goreniya Vzryva* **12** (5), 754–758 (1976) [*Combust., Expl., Shock Waves* **12** (5), 675–758 (1976)].
13. B. G. Loboiko and S. N. Lubyatinsky, "Reaction Zones of Detonating Solid Explosives," *Fiz. Goreniya Vzryva* **36** (6), 45–64 (2000) [*Combust., Expl., Shock Waves* **36** (6), 716–733 (2000)].